Mechanics & Industry **22**, 46 (2021)
© L. Zhang et al., Published by EDP Sciences 2021
https://doi.org/10.1051/meca/2021046

Mechanics & Industry

Available online at:
www.mechanics-industry.org

REGULAR ARTICLE

OPEN ACCESS

Effects of stable clearances on backflow in the variable-pitch screw vacuum pump

Li Zhang*, Yongju Zhang, and Ziyun Chen

School of Intelligent Manufacture, Taizhou University, Taizhou, Zhejiang 318000, China

Received: 13 April 2021 / Accepted: 22 October 2021

Abstract. Effects of various clearances of variable-pitch screw vacuum pump on gas backflow of internal flow field of the pump cavity is studied. The theoretical tooth surfaces of screw rotor are optimized by radial, normal equidistance modifications, and four types of stable clearances of rotor circumferential, radial, tooth shape and tooth sides are obtained. The backflow calculation model in clearances considering Couette backflow and orifice backflow is improved. The three-dimensional model of variable-pitch screw vacuum pump is designed, and the experimental prototype and test device are developed. The internal backflow of vacuum pump is analyzed by using the commercial software Ansys-Fluent® and the calculation model. The results show that the smaller the clearances, the smaller the backflow and the higher the vacuum degree. Among the four types of clearances, the circumferential clearance plays the primary roles. The backflow is directly proportional to the inlet pressure and rotating speed. Predictions are validated by the experimental data with satisfied agreement.

Keywords: Variable-pitch / screw vacuum pump / stable clearances / backflow / interstage / numerical simulation

1 Introduction

The screw vacuum pump is a kind of dry vacuum acquisition equipment. The operating point of the vacuum pump has been changing continuously the pressure in the container to the target pressure via transferring gas from inlet side to outlet side. In recent years, internal compression technology of the variable-pitch screw vacuum pump is widely used in the field of metallurgical, pharmaceutical, chemical and semiconductor industries because of the advantages of high pumping speed and low energy consumption [1]. The screw rotors are the most critical and complex part for this kind of vacuum pump [2,3]. A pair of meshing conjugated male and female rotors in the pump cavity rotate in opposite directions, driving the gas to complete the suction, compression and discharge processes between stages through the clearances in the cavity. To prevent the interference by screw rotor thermal expansion during the operations, clearances between female and male screw rotors, as well as rotors and stator should be considered accurately. The backflow moving from the high-pressure side to low-pressure side through clearances is generated when the gas went through the pump volume. It takes great effect on the performance of pump, such as the ultimate vacuum etc.

Ohbayshi et al. [4] proposed a performance prediction algorithm to investigate the performance by means of the balance among geometrical pumping speed, net output and leaks. Rabiger et al. [5] established a finite volume model to analyze the distributions of velocity, pressure and temperature of the twin-screw pump clearances using numerical simulation method. Fong et al. [6] presented the shape and size of the clearance path to calculate the clearances of rotors. Ryazantsev et al. [7] built the relationship between screw clearance and deflection. Li et al. [8] studied the gas flow state of the constant pitch screw vacuum pump, and disclosed the influence of different clearances and screw rotor parameters on the backflow. Sham et al. [9] proposed an algebraic grid generation algorithm for unstructured grid, and described Finite Volume Method (FVM) for variable-pitch and variable profile screw machines. Also, they compared the CFD results of constant pitch rotors, variable-pitch rotors and variable profile rotors. Xiao et al. 2017 [10] calculated the mass flow leakage of constant pitch screw vacuum pump and they found that each leakage path has different impacts on the pumping speed and total leakage rate. Jerry et al. [11] provided the results of bench-scale testing of Archimedes hydrodynamic screw three-dimensional

* e-mail: yushugen@tzc.edu.cn

printed models, and they evaluate the performance of various shapes and parameters for Archimedes hydrodynamic screws. Zöllig [12] used dry compressing screw vacuum pumps and Roots pumps to the degassing process, and the performance research shown that the energy consumption of variable-pitch rotor was lower. Abhay et al. [13] investigated the effect of heat generation during the period of wet gas compression on the pump performance and potential mitigation measures to consequential issues for fixed flow rate of seal flush-fluid recirculation. Wu et al. [14] estimated the meshing line clearance using normal tooth surface by cross-section profile of rotor. Dirk et al. [15] presented detailed analyses of the operating performance of a dry-running screw vacuum pump, and they used experimental and theoretical methods to research characteristic parameters, suction speed and final attainable pressure of screw pump. Zhao et al. [16] proposed the thermodynamic procedures for four distinctive processes, including sucking, transferring, backlashing and exhausting process. Kauder et al. [17] researched the influence of the different parameters of screw pump on the delivery rate, volume flow rate and the specific power, such as rotor crown, root diameter, number of lobes and rotor gradient. Pfaller et al. [18] established the calculation method of chamber pressures and mass flows of dry-running screw pump, and illustrated the relationship among working chamber volumes, stage pressure rations and isentropic compression work for different suction pressures. Burmistrov et al. [19] used the angular coefficients method to calculate the conductance of channels with more complicated profiles, such as in Roots pumps working in the molecular flow regime. Stosic et al. [20] used the standard screw compressor design software to create a series of rotor profiles of vacuum and multiphase pumps, and carried out performances calculations on them. Salikeev et al. [21] defined the conductance of channels of vacuum and compressor, which formed by cylindrical walls and of rectangular channels, in a wide range of geometrical dimensions, inlet pressures and pressure ratios with Navier-Stokes equations system. Salikeev et al. [22] calculated conductance coefficients of slot channels formed by cylindrical walls by Monte Carlo method with different wall radius and clearances. Salikeev et al. [23] presented the relationship of conductance calculation using three types of slot channels in viscous flow regime at small pressure differences at the ends of the channel. Salikeev et al. [24] presented a method for prompt conductance calculation of slot channels with the minimal clearance at a certain point along gas flow direction, and it was used in mathematical models for the pumping process of scroll pumps, claw pumps and Roots pumps.

To date, the studies on the flow field performance of vacuum pump mainly focus on the fixed pitch screw vacuum pump and Roots pump, in regards with studies of the variable-pitch screw vacuum pump are fewer. Ohbayshi et al. [4] estimated the backflows of fixed pitch screw vacuum pump, backflows in interstage clearances, as well as their effects on performance. However, the detailed hydrodynamic information was neglected. Thus, it is very important to fully consider the gas backflow among interstage clearances for predicting the performance

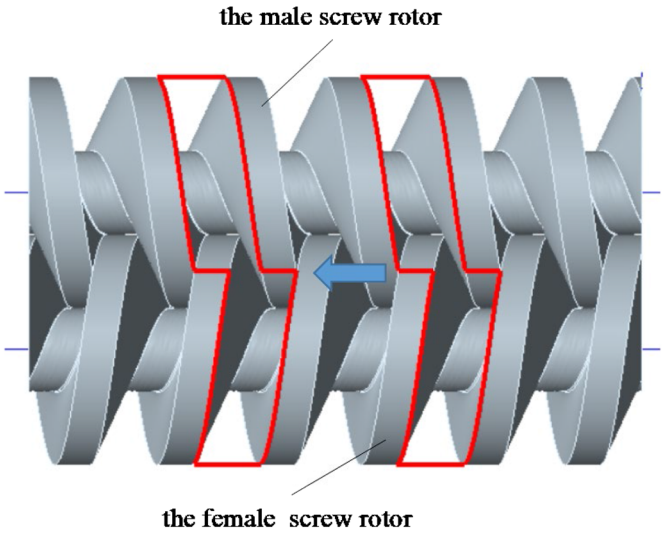

Fig. 1. Fixed pitch screw vacuum pump.

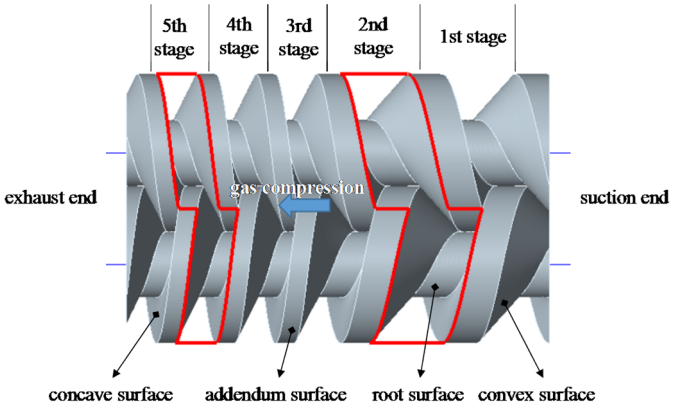

Fig. 2. Schematic diagram of theoretical variable-pitch screw rotor.

parameters of pump and reasonable designations of clearance among rotors. As shown in Figures 1 and 2, compared to those of the fixed screw vacuum pump, the roles of the variable-pitch screw vacuum pump have been changed, which make the gas compression and the areas of backflow are changeable. As a result, backflow among interstage clearances is different and it takes great effect on the pumping speed and limitation vacuum. In this work, an improved calculation model to describe the backflow in variable-pitch screw vacuum pump is developed. Stable clearances are obtained by modifying theoretical tooth surfaces of the screw rotor, and the effects of clearances on backflow are discussed. Experimental validations for proposed model and algorithm are acceptable.

2 Stable clearances generation in the screw pump

According to the theoretical design, a pair of screw rotors without meshing clearances are obtained (see Fig. 2).

The addendum surface, root surface, concave surface and convex surface are the theoretical tooth surfaces. The suction end is set to the first stage, and the exhaust end is set to the fifth stage. Clearances are the important parameters to ensure better performances for the pump. Generally, the clearances are required to be evenly distributed from exhaust to suction ends. Since uneven clearances deteriorate the stability of vacuum pump operation and internal gas flow characteristics, therefore, the design for clearances are strategies and challenges. In order to obtain predetermined and stable clearances, this paper references Zhang's method [25] to carry out equidistant modification on the theoretical tooth surface. Based on the different paths of theoretical tooth surface modifications, this method is classified into two ways, that is the addendum and root surfaces using radial equidistant modification, the concave and convex surfaces using normal equidistant modification.

2.1 Radial equidistant modification

Theoretical tooth surface is shifted a small distance to the center along with diameter direction to acquire a predetermined clearance, equation is given as follows:

$$\begin{cases} x_r(t) = x(t) - \delta/2 \\ y_r(t) = y(t) - \delta/2. \end{cases} \tag{1}$$

Radial equidistant modification of root surface is given in Figure 3, and modified equations is represented as below

See equation (2) below.

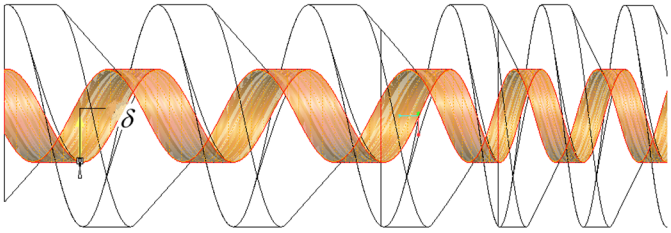

Fig. 3. Modified root surface.

Modified equations of the radial equidistant addendum surface are described by

See equation (3) below.

2.2 Normal equidistant modification

Theoretical tooth surface is shifted a small distance to the center along with normal direction to obtain a predetermined clearance, equation is given as

$$\begin{cases} x_r(t) = x(t) - \delta \sin\gamma \\ y_r(t) = y(t) - \delta \cos\gamma. \end{cases} \tag{4}$$

Normal equidistant modification of concave surface is given as Figure 4, modified equation is

See equation (5) below.

$$\begin{cases} x_r(t) = \left(R_F - \dfrac{\delta_2+\delta_1}{2}\right)\cos\left(\left(\sqrt{\left(\dfrac{R_F}{R_0}\right)^2 - 1} - \arctan\sqrt{\left(\dfrac{R_F}{R_0}\right)^2 - 1} + \pi - \sqrt{\left(\dfrac{R_d}{R_0}\right)^2 - 1} + \arctan\sqrt{\left(\dfrac{R_d}{R_0}\right)^2 - 1}\right)t\right) \\ y_r(t) = \left(R_F - \dfrac{\delta_2+\delta_1}{2}\right)\sin\left(\left(\sqrt{\left(\dfrac{R_F}{R_0}\right)^2 - 1} - \arctan\sqrt{\left(\dfrac{R_F}{R_0}\right)^2 - 1} + \pi - \sqrt{\left(\dfrac{R_d}{R_0}\right)^2 - 1} + \arctan\sqrt{\left(\dfrac{R_d}{R_0}\right)^2 - 1}\right)t\right) \end{cases} \tag{2}$$

$$\begin{cases} x_r(t) = \left(R_A - \dfrac{\delta_1}{2}\right)\cos\left(\left(\sqrt{\left(\dfrac{R_A}{R_0}\right)^2 - 1} - \arctan\sqrt{\left(\dfrac{R_A}{R_0}\right)^2 - 1} + \pi - \sqrt{\left(\dfrac{R_d}{R_0}\right)^2 - 1} + \arctan\sqrt{\left(\dfrac{R_d}{R_0}\right)^2 - 1}\right)t\right) \\ y_r(t) = \left(R_A - \dfrac{\delta_1}{2}\right)\sin\left(\left(\sqrt{\left(\dfrac{R_A}{R_0}\right)^2 - 1} - \arctan\sqrt{\left(\dfrac{R_A}{R_0}\right)^2 - 1} + \pi - \sqrt{\left(\dfrac{R_d}{R_0}\right)^2 - 1} + \arctan\sqrt{\left(\dfrac{R_d}{R_0}\right)^2 - 1}\right)t\right) \end{cases} \tag{3}$$

$$\begin{cases} x_r(t) = (R_F + R_A)\cos\left(\arccos\left(\dfrac{R_d}{R_A}\right)t\right) - R_A\cos\left(2\arccos\left(\dfrac{R_d}{R_A}\right)t\right) \pm \dfrac{\delta_3}{2}\sin\gamma \\ y_r(t) = (R_F + R_A)\sin\left(2\arccos\left(\dfrac{R_d}{R_A}\right)t\right) - R_A\sin\left(2\arccos\left(\dfrac{R_d}{R_A}\right)t\right) - \dfrac{\delta_3}{2}\cos\gamma \end{cases} \tag{5}$$

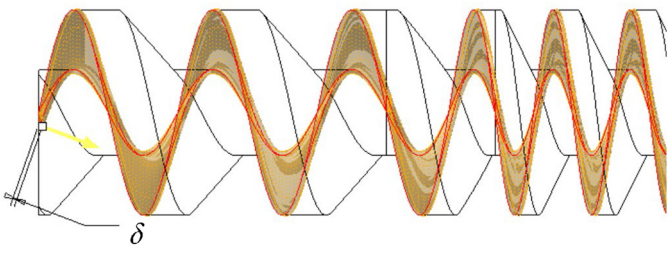

Fig. 4. Modified concave surface.

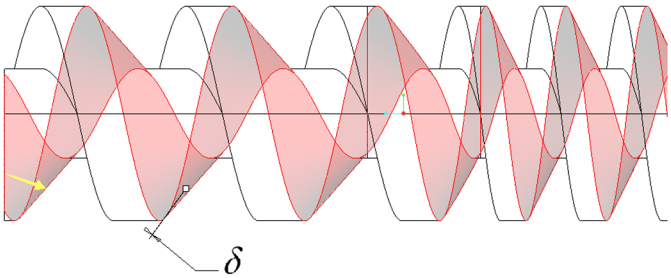

Fig. 5. Modified convex surface.

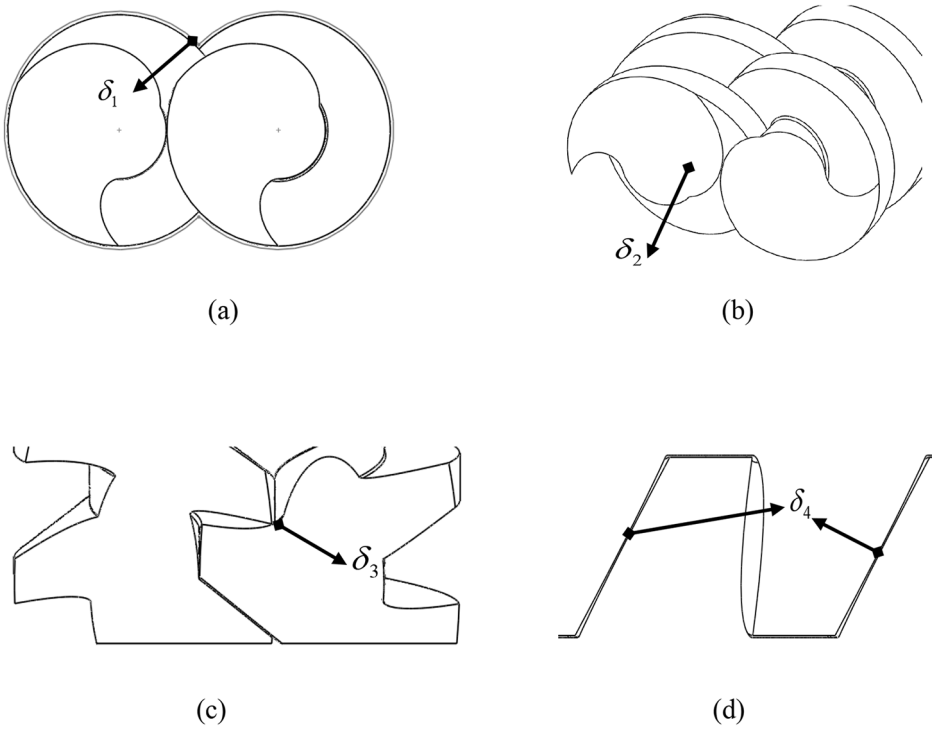

Fig. 6. Four types of clearances: (a) circumferential clearance; (b) radial clearance; (c) tooth side clearance; (d) the tooth shape clearance.

where, if $0 \leq \arccos(\frac{R_d}{R_A}) \leq 90, \pm$ is the negative, if $90 < \arccos(\frac{R_d}{R_A}) \leq 180, \pm$ is the positive, $\gamma = \arctan\frac{x(t)}{y(t)}$.

Normal equidistant modification of convex surface is given in Figure 5, modified equation is

See equation (6) below.

where, $\tilde{R} \in [R_F, R_A]$, if $y_r(t) > 0, \pm$ is the negative, otherwise it is the positive, $\vartheta = \arctan\frac{x(t)}{y(t)}$.

Figure 6 shows the distributions of the clearances after modification, the circumferential clearance of cylindrical wedge, and other three types of clearance by nozzle slits.

3 Calculation model of backflow in clearances

3.1 Areas of various clearances

The following areas of each clearances are

$$A_1 = 2\left(1 - \frac{1}{\pi}\arccos\frac{R_d}{R_A}\right)\sqrt{(2\pi R_A)^2 + (S^N)^2}\delta_1 \tag{7}$$

$$A_2^j = 2B^j\delta_2 \tag{8}$$

$$\begin{cases} x_r(t) = R_0(\cos(\sqrt{(\tilde{R}(t)/R_0)^2 - 1} + \beta) + \sqrt{(\tilde{R}(t)/R_0)^2 - 1} * \sin(\sqrt{(\tilde{R}(t)/R_0)^2 - 1} + \beta)) + \dfrac{\delta_4}{2}\sin\vartheta \\ y_r(t) = R_0(\sin(\sqrt{(\tilde{R}(t)/R_0)^2 - 1} + \beta) + \sqrt{(\tilde{R}(t)/R_0)^2 - 1} * \cos(\sqrt{(\tilde{R}(t)/R_0)^2 - 1} + \beta)) \pm \dfrac{\delta_4}{2}\cos\vartheta \end{cases} \tag{6}$$

$$A_3^j = \frac{R_A - R_F}{\cos\beta^j}\delta_3 \tag{9}$$

$$A_4^j = \sqrt{(R_A - R_F)^2 + (S^j - 2B^j)^2}\delta_4. \tag{10}$$

3.2 Backflow calculation model of various types of clearances

The derivation of the calculation model is based on the following assumptions:
– Gas in the pump cavity is ideal gas.
– Gas heat exchanges between cavity and body are neglected.

Backflow has the complicated relationships with clearance areas, working temperature, interstage pressure, movement mode of the two parts, and relevant structural dimensions of each stages. Based on the Ohbayshi [4] and Da [26], the backflow calculation model in this paper is deduced. Backflow through these clearances can be considered to be the Couette flow and orifice effect flow, which Couette backflow is caused by the relative motion between rotors and between rotor and stator, and the orifice backflow is caused by the gas passing through the thin-walled small hole.

Couette backflow of the jth interstage clearance in the ith type clearance is

$$\tilde{M}_{ci}^j = v_i A_i^j \sin\beta^j P^j = v_i A_i^j \sin\left(\arctan\left(\frac{S^j}{2\pi R_A}\right)\right)P^j. \tag{11}$$

The orifice backflow of the jth interstage clearance in the ith type clearance is

$$\tilde{M}_{si}^j = \sqrt{\frac{2K}{K-1}\frac{RT}{\mu}(1 - x^{\frac{K-1}{K}})x^{\frac{1}{K}}}P^j A_i^j. \tag{12}$$

Backflow of the jth interstage clearance in the ith type clearance is

$$\tilde{M}_i^j = \tilde{M}_{ci}^j + \tilde{M}_{si}^j. \tag{13}$$

Total backflow of the jth interstage clearance is

$$\tilde{M}^j = \sum_{i=1}^{4}\tilde{M}_i^j\Big|_{j=[1,N]}. \tag{14}$$

4 Experimental settings and numerical simulation

4.1 Physical description

The vacuum pump discussed in this paper has the same basic structure and geometric dimensions, as shown in Table 1. Three kinds of the vacuum pumps with different clearance sizes are designed within the tolerance range, the constraints of thermal expansion and other factors accordingly, that called the large clearance screw vacuum pump (LCSVP), the middle clearance screw vacuum pump (MCSVP), and the small clearance screw vacuum pump (SCSVP). LCSVP and MCSVP only have different circumferential clearance, their radial, tooth side and tooth profile clearances are the same. The circumferential, radial and tooth clearance of SCSVP are small. Clearance sizes are shown in Figure 7.

Table 1. Dimensions of variable-pitch screw vacuum pump.

Design parameter	Dimension
Addendum circle diameter	148 mm
Root circle diameter	62 mm
Pitch circle diameter	52.5 mm
Rotor length	398 mm
Distance between two axis	105 mm
Exhaust end pitch	56 mm
Suction end pitch	101 mm
The number of turns	5.5

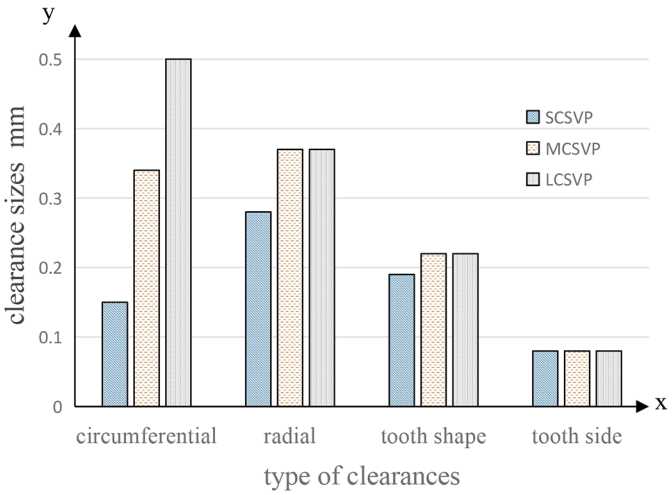

Fig. 7. Different clearance sizes of three kinds of vacuum pumps.

4.2 Experimental settings

Main purpose of experiment is to validate the proposed theoretical model and numerical simulation results. SCSVP is used as the test sample, and the interstage pressures with different inlet pressure values is the fundamental parameter. The test device is shown in Figure 8. Pressure in the vacuum cover and pump is measured by the pressure sensor. There are five small holes on the side of the SCSVP, and the five pressure sensors are installed in these holes to measure the pressure. Pressure sensor model is PVG 550 with range from 0.01 Pa to 150,000 Pa. The reading accuracy of ±1% corresponds to the 3000–150000Pa, and ±5% is for the 0.1–3000 Pa and ±10% is for the 0.01–0.1Pa, respectively. The test

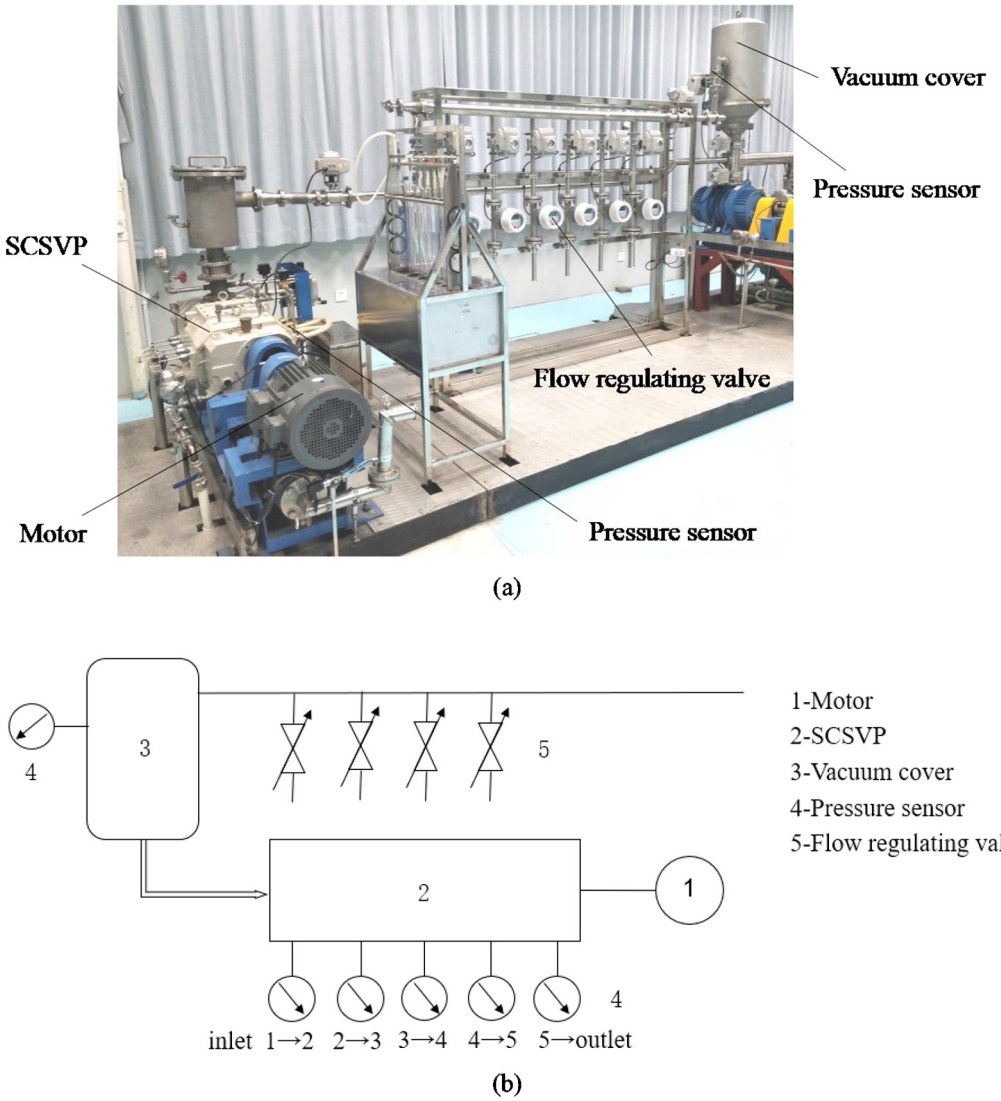

Fig. 8. The test platform of screw vacuum pump (a) and its schematic design (b).

Table 2. Experimental data.

Pressure of vacuum cover Pa	Flow regulating value reading m^3/h	Interstage pressure of SCSVP Pa					Capacity of suction Pa.m^3/s
		1→2	2→3	3→4	4→5	5→outlet	
861	0.70	861	2414	3602	19049	111316	19.80
508	0.34	508	2023	3365	17959	111100	9.65
293	0.18	293	1907	3317	17477	111316	5.07
178	0.05	178	1840	3200	17263	111316	1.41
96	0.015	96	1800	3371	17854	111533	0.41

vacuum pump is driven by a motor. By adjusting the flow regulating valve, a small amount of air is pushed into the vacuum cover to maintain the pressure at a stable value in the cover leading to the stable pressure under the corresponding working conditions. The model of flow regulating valve is LZD-25/R4 /M8/ESK-Z/G with range of 0–0.7 m^3/h, 0–7 m^3/h, 0–70 m^3/h, 0–150 m^3/h, and reading accuracy is ±1.5%. The experimental data are automatically collected by the measurement system.

When the pressure at vacuum cover reaches up to a stable value, record the experimental test data, as shown in Table 2. Acquirement data mainly include interstage pressure and gas flow velocity at the inlet of flow regulating value.

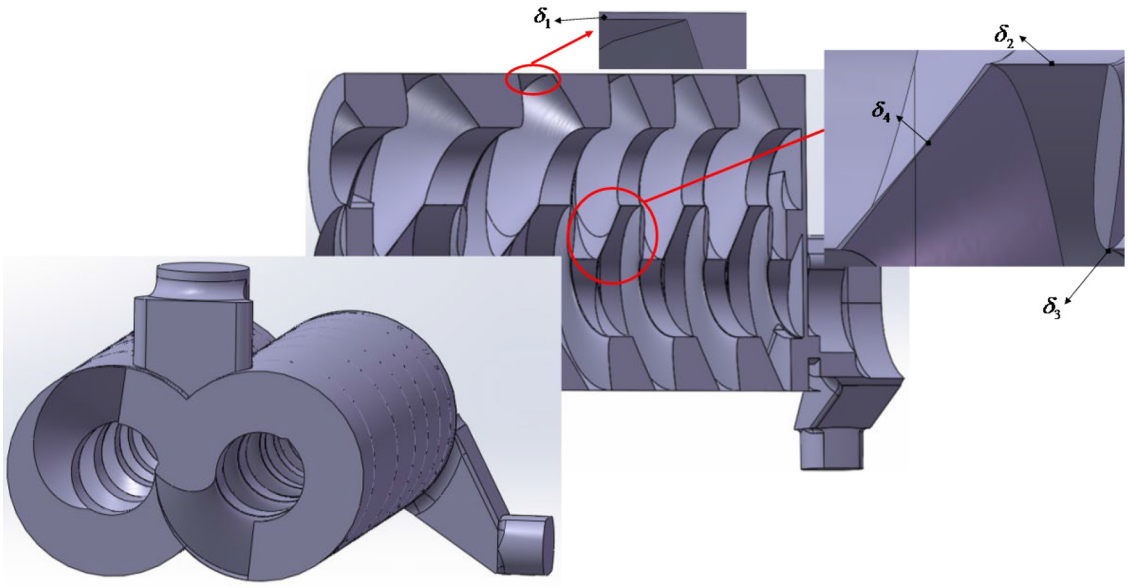

Fig. 9. Fluid domain of screw vacuum pump.

4.3 Numerical simulation

After assembling the screw rotors, stator, plate and exhaust end, the 3D model of screw vacuum pump is generated. The grid system and calculation domain using commercial software ANSYS are shown in Figure 9, which is divided into the main flow field and the clearance flow field. The clearance flow field is marked in Figure 9.

The fluid domain is divided by unstructured meshes and k-ε two-equation model is used as the governing equations. The semi-implicit pressure linked equations-corrected (SIMPLEC) algorithm to correct p-v correlation with tri-diagonal marching algorithm (TDMA) line-by-line iteration, under-relaxation quadratic upstream interpolation, convective kinematics (QUICK) procedure and the central difference scheme (CDS) for the diffusion terms are made for the solution of the finite differential equations. The pressure boundary condition is set to the inlet and outlet, and the velocity boundary condition is set to the outer surface of the rotors. The boundary conditions are listed as follows: the series values of inlet pressure are 96 Pa, 178 Pa, 293 Pa, 508 Pa and 861 Pa, exit pressure is about 101,325 Pa, the female screw rotor speed is approximately 2,900 r/min, the male screw rotor speed is 2,900 r/min, respectively.

4.4 Fluid domain grids settings

The inlet pressure is set to 861 Pa. Under the same other boundary conditions, three grid sizes are used for numerical simulation. The flow velocity vector diagram of the three grids is shown in Figure 10 and the simulation results are shown in Table 3. The maximum flow velocity error range of medium grid and fine grid is 2.22%, and that of coarse grid and fine grid is 7.98%. It shows that the grid has good independence.

In Table 3, the simulated pumping speed in the last column is obtained by multiplying the flow velocity in the fourth column by the circumferential clearance area. The actual pumping speed is obtained by the pressure of vacuum cover in the first column and the flow regulating value reading in the second column of Table 2. The actual pumping speed at inlet pressure of 861Pa is

$$S_{ac} = \frac{0.7 \times 101325}{861 \times 3600} = 0.023\mathrm{m}^3/\mathrm{s}.$$

By comparing the pumping speed values of simulation analysis and actual test, and comprehensively considering the simulation solution accuracy and iteration time, the medium grid is used to mesh the fluid domain.

Pressure distribution diagram of the fluid domain is obtained in Figure 11. The warm color represents high pressure and the cold color represents low pressure. It can be seen from the figure that the inlet pressure is low and the pressure in the cavity gradually increases from the suction end to the exhaust end.

The flow velocity vector diagram of the three pumps is shown in Figure 12. The warm color represents high flow velocity and the cold color represents low flow velocity. In the figure, the gas in the adjacent pump chamber moves from the suction end to the exhaust end under the action of rotors movement. The flow velocity of LCSVP is the largest, MCSVP is the second, and SCSVP is the smallest. In the enlarged figure, we can see the phenomenon of backflow from the high-pressure chamber to the low-pressure chamber.

5 Result and discussions

Using the calculation model equation (14) and selecting the same boundary parameters as the numerical simulation,

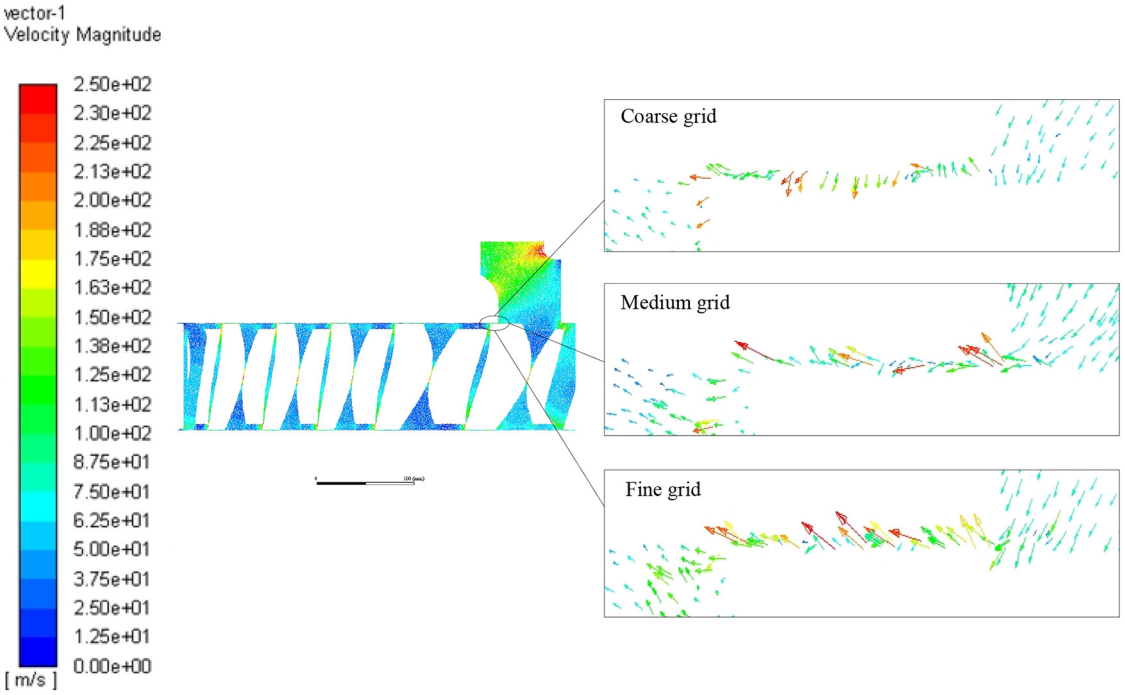

Fig. 10. The flow velocity vector diagram of the three grids.

Table 3. The grid of fluid domain.

Type	Number	Min mesh mm	Max mesh mm	Iteration time S	The maximum flow velocity m/s	The simulated pumping speed m^3/s
Coarse grid	12246318	4.2E–2	1.65	3520	213	0.022
Medium grid	13412142	3.2E–2	1.6	3776	225	0.024
Fine grid	14733566	3.2E–2	1.55	4248	230	0.024

the theoretical calculation value of backflow can be obtained.

5.1 Effects of clearance sizes

The calculation results of interstage backflow of the three pumps are shown in Figure 13. We can see that the total backflow of the pump with small clearance is also small. And the backflow of LCSVP from 1st to 5th stages are approximately 2.8–3.0 times larger than that of SCSVP. The backflow from 5th to 1st stages changes from large to small, because as the clearance channel of the flow field goes deeper to the suction end, the more the backflow gas is blocked. From the specific values, the backflow from 5th to 4th decreased by 85.4% and it decreased by 79.7% once more from 4th to 3th, indicating that the three stages play very important role for backflow interceptions. Therefore, in order to obtain higher vacuum, more rotor stages need to be designed, usually exceed in 5 stages.

The smaller clearances with the same rotor stages make contribution to getting the higher vacuum degree. However, the stuck phenomenon caused by thermal expansion for smaller clearance pump is an fatal factor for operation. Therefore, in the actual design of vacuum pump products, it is important to reasonably select the rotor stages and clearances. The experimental test results of the prototype show that the ultimate vacuum of MCSVP is 18 Pa and that of SCSVP is 5 Pa, which is consistent with the above analysis results.

5.2 Effects of clearance types on 1st stage backflow

Since 1st stage gas pressure is closest to the actual vacuum working environment, it is reasonable to select 1st stage backflow as the marking object. The influence of various clearances on 1st stage backflow is analyzed.

In order to facilitate the comparison with the experimental results, the 96 Pa inlet pressure actually obtained during the experiment is selected as the inlet pressure value set in the calculation. The relationship curves between 1st stage backflow with the four types of clearance are obtained through equation (14), as shown in Figure 14. We found that, firstly, the change trends of LCSVP, MCSVP and SCSVP are consistent. Secondly,

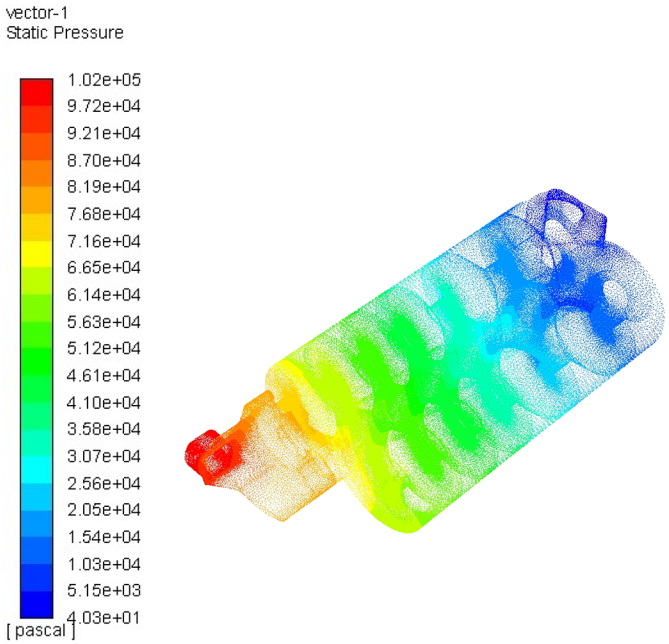

Fig. 11. Pressure distribution diagram of the fluid domain.

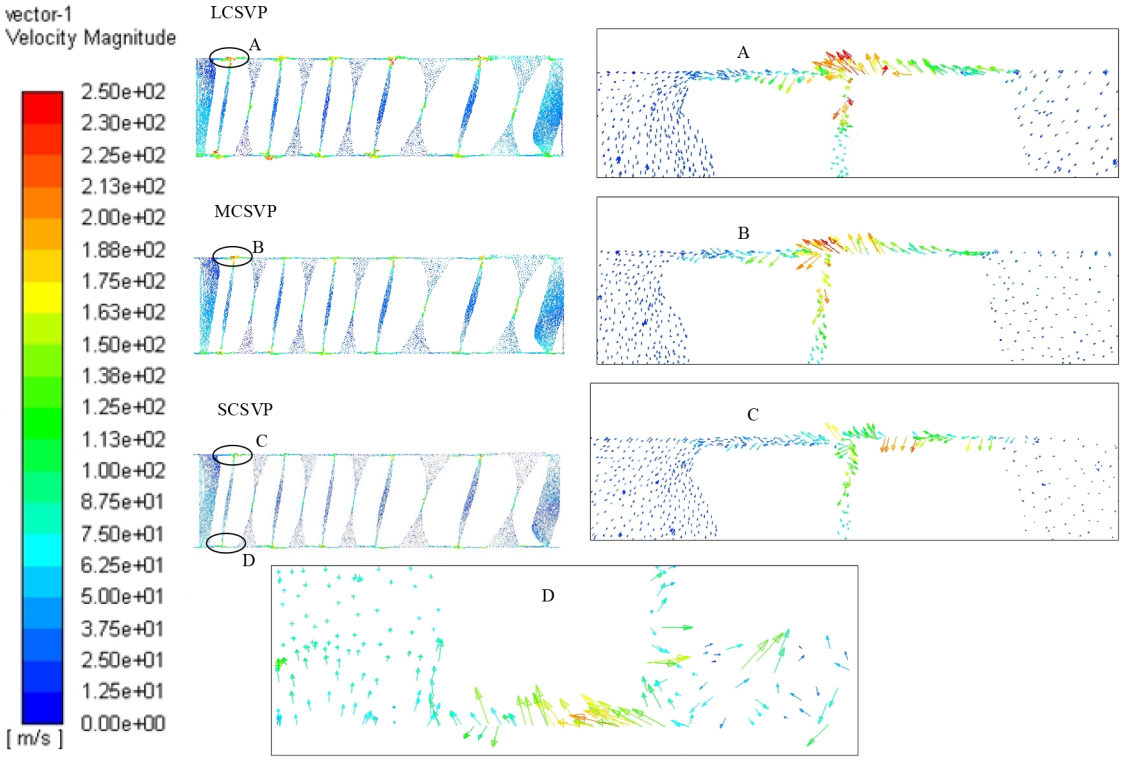

Fig. 12. The flow velocity vector diagram of the three pumps.

circumferential clearances have the approximately 80% contributions to backflow in comparisons with the other three types of clearances, and the backflow of radial clearance, tooth side clearance and tooth profile clearance is much smaller. This is because the circumferential clearance is a kind of cylindrical wedge with largest area in clearance channel, and the backflow is directly proportional to the area of the clearance channel. The calculation result shows that the backflow of LCSVP is approximately 3.3 times larger than that of SCSVP. In the enlarged figure, it can be seen that the curves of LCSVP and MCSVP are coincided. It can be explained that

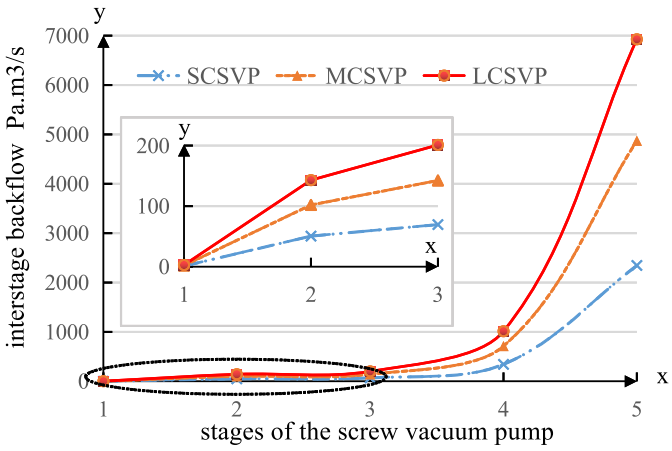

Fig. 13. The influence of clearance size on the interstage backflow.

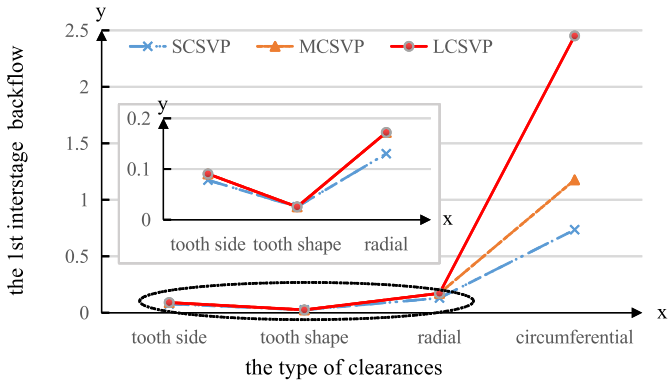

Fig. 14. Comparison of 1st stage backflow between four types of clearances.

clearance sizes of the radial, tooth side and tooth shape of the two pumps are the same (see Fig. 7), and the backflow is consistent.

Because the circumferential clearance has a great influence on backflow, so it is specially studied here. Figure 15 shows the relationship curves between the inlet pressure and 1st stage backflow with different circumferential clearances of LCSVP, MCSVP and SCSVP. The simulated backflow data obtained from equation (11) is the product of 1st stage pressure, the simulated flow velocity and the circumferential clearance cross-sectional area. It can be seen that the theoretical calculation results is in good agreement with the numerical simulation results. And the changes of backflow between 1st stage and inlet pressure maintains the same trend and are in directly proportion. The backflow of LCSVP changes most violently with the inlet pressure. When the inlet pressure decreases from 816 Pa to 96 Pa, the backflow decreases from 57 Pa.m^3/s to 2.45 Pa.m^3/s.

Due to the significant influence of circumferential clearance, its design is the key. During the operation of variable-pitch screw vacuum pump, as the gas is continuously transported and compressed in the pump cavity, the

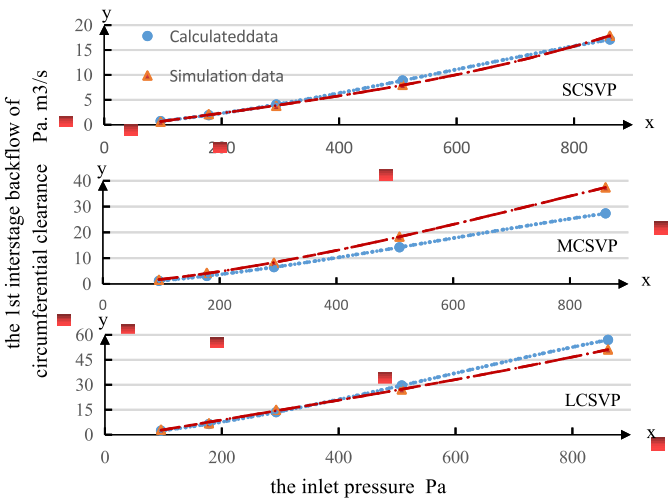

Fig. 15. Relationship between the 1st interstage backflow of circumferential clearance and inlet pressure.

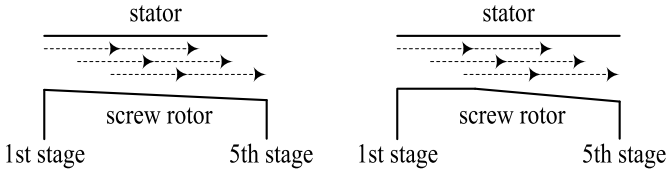

Fig. 16. Two variable distance gradient design for circumferential clearance.

temperature of vacuum pump from suction end to exhaust end increases continuously, that is, the thermal expansion of screw rotor and stator is also that the exhaust end is greater than the suction end. In order to obtain a higher vacuum degree by controlling the backflow, a better design is to gradually reduce the circumferential clearance from 5th stage to 1st stage, as shown in Figure 16. This design can avoid the stuck of rotors by the thermal expansion, and can block more backflow gas near the suction end due to a small clearance, so as to obtain a higher vacuum degree. Therefore, variable distance gradient design should be adopted for circumferential clearance in product design. Figure 16 shows two different gradient changes in design.

5.3 Effects of clearance length

It is not only the circumferential clearance's cross-sectional area that affects the backflow, but also the its length, as shown in Figure 17. When the circumferential clearance length increases, the change trends of LCSVP, MCSVP and SCSVP are the same, and the total backflow decreases with the increase of clearance length. The longer the clearance length is, the longer the clearance channel is formed, and the more the backflow gas is blocked. When the clearance length increases from 16 mm to 20 mm, the interstage backflow decreases accordingly. The decline curves of the three pumps are shown in Figure 18. Maximum decrement occurs at SCSVP and smaller

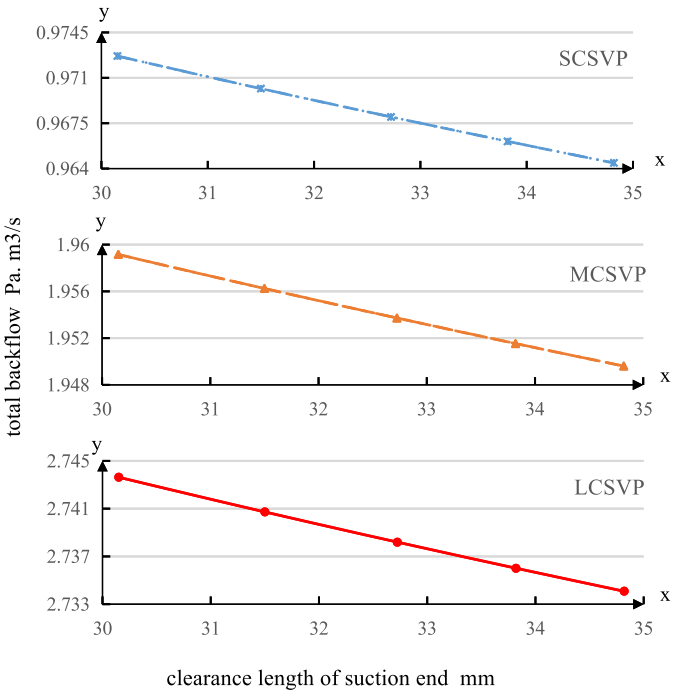

Fig. 17. Effects of clearance length on total backflow.

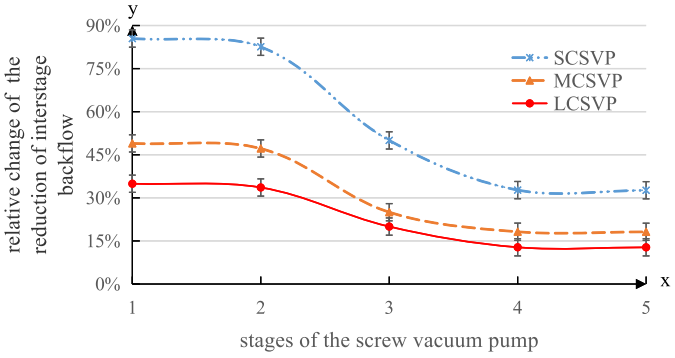

Fig. 18. The decline curves of interstage backflow at different clearances lengths.

decrements are for LCSVP and MCSVP. Those of LCSVP and MCSVP decreased by 40.8% and 57.3%, respectively. As far as it concerns for vacuum pump, the circumferential clearance length takes a great effect on the backflow on the conditions that the smaller clearances. Therefore, when designing screw rotor, the circumferential clearance length cannot be too small.

5.4 Effects of inlet pressure

Figure 19 shows the correlation between inlet pressure and the total backflow. When the total backflow increases, more gas returns to the suction end. Under the condition of maintaining a certain pumping flow, the inlet pressure increases and the vacuum degree decreases. When inlet pressure increased from 96 Pa to 861 Pa, the increment of

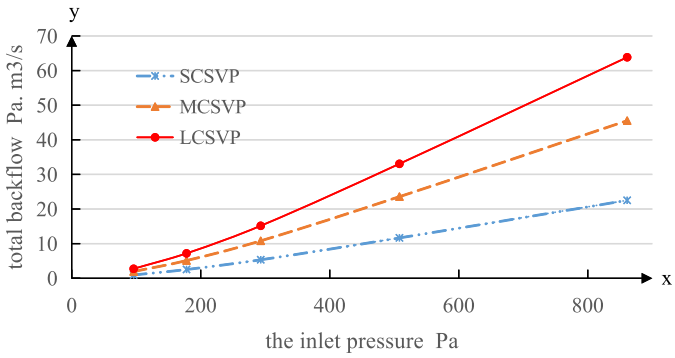

Fig. 19. Effects of inlet pressure on total backflow.

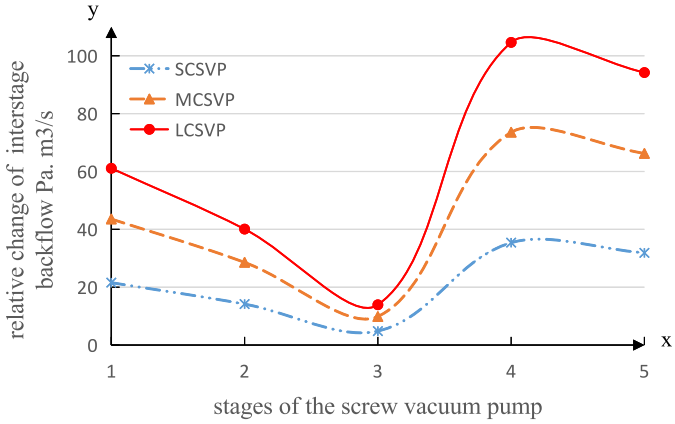

Fig. 20. Curves of interstage backflow increment with inlet pressure.

the total backflow of LCSVP is 64.6% of SCSVP and 28.6% of MCSVP. The results show that with the increase of inlet pressure, the increment of the backflow has a nonlinear relationship with the clearance. When the clearance increases to a certain extent, the increment of the backflow slows down. Figure 20 shows the increment curve of the interstage backflow with inlet pressure. When the inlet pressure rises from 96 Pa to 861 Pa, the increment of the interstage backflow of the three pumps generally presents a saddle shape, which is significantly different from the equidistant screw vacuum pump. As can be seen from the figure, the increment of the 3rd stage backflow is the smallest. This is because the 3rd stage is a variable pitch section, and the gas is compressed in this section, so that the pressure in the front and rear sections of the 3rd stage changes little. It just reflects the internal compression characteristics of the variable pitch screw vacuum pump. The 4th stage is close to the exhaust end and is greatly affected by the outlet pressure, resulting in the most obvious increase of the 4th stage backflow.

5.5 Effects of rotating speed

Figure 21 shows the correlation curves between rotating speed and the total backflow. When the rotating speed increases, the change trends of LCSVP, MCSVP and

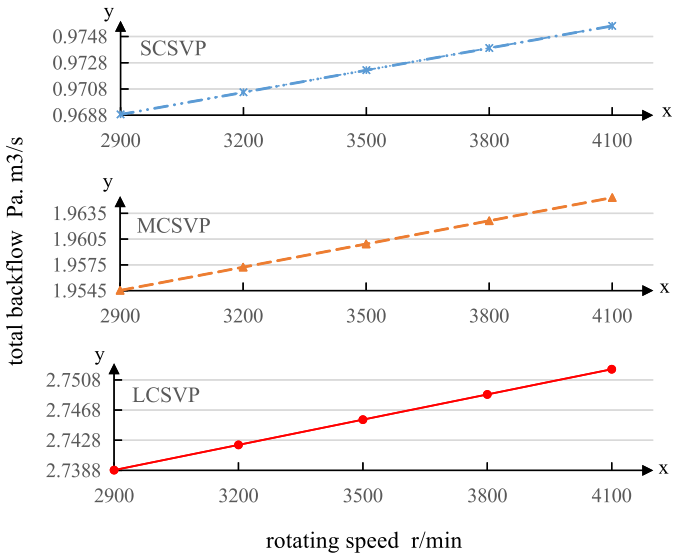

Fig. 21. Effects of rotating speed on total backflow.

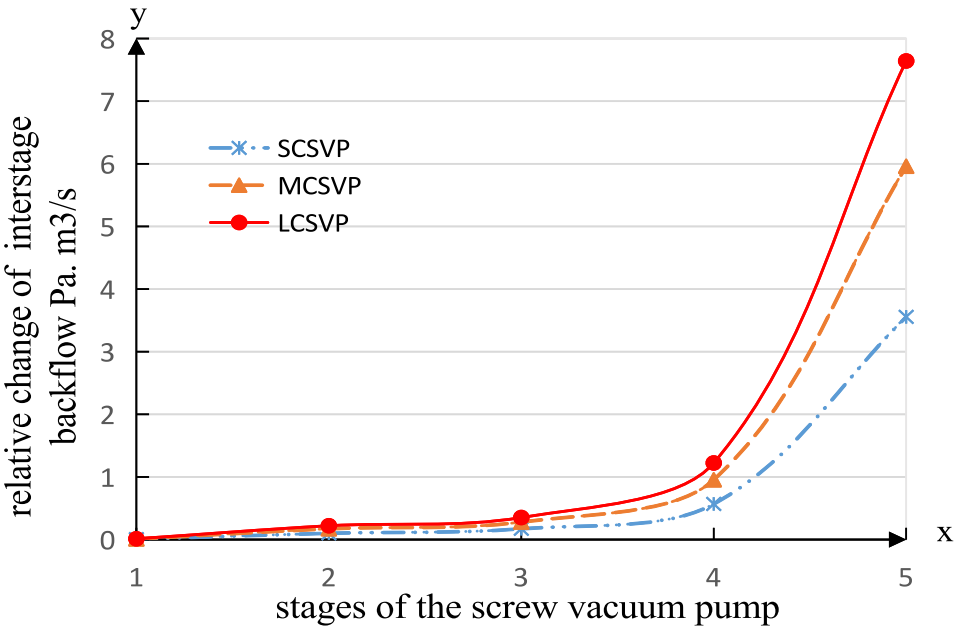

Fig. 22. Curves of interstage backflow increment with rotating speed.

SCSVP are the same. Rotating speed is directly proportional to the total backflow, vice versa. This is because when the rotating speed is higher and the pumping speed is higher, the gas flow increases, the interstage pressure difference increases, and the backflow increases. The increment curve of interstage backflow are shown in Figure 22 as rotating speed ranging from 2900 r/min to 4100 r/min. The increment of 5th stage is the largest, the increment of LCSVP is about 53.5% larger than that of SCSVP, and the increment of MCSVP is about 40.3% larger than that of SCSVP. This is because 5th stage is located at the exhaust end, the backflow is relatively large. The Couette backflow is directly proportional to the rotating speed, and increase of the rotating speed leads to intensification of the backflow. Therefore, the rotating speed change has an obvious influence on the increment of the interstage backflow near the exhaust end.

5.6 Experimental results and comparison

When the pressure at vacuum cover reaches up to a stable value, gas balance in vacuum system is achieved. The experimental test results are shown in Table 2. The data of pumping speed in the last column is obtained by converting the actual pressure in the first column and the flow velocity measured in the second column. Since the vacuum system

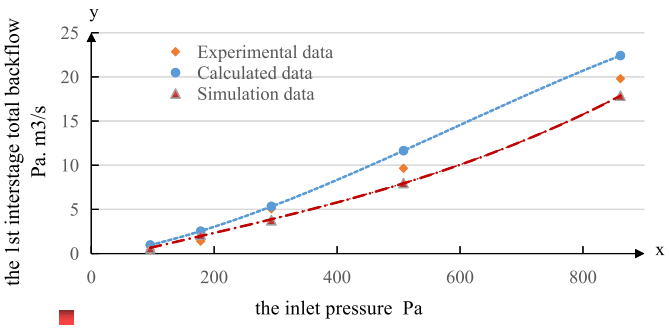

Fig. 23. Comparisons of three methods of the 1st interstage total backflow in SCSVP.

is in equilibrium at this time, the pumping speed obtained by experimental measurement is the total backflow, that is, the 1st stage backflow.

According to the experimental data in Table 2, the comparison results with the numerical simulation and model calculation above are shown in Figure 23. As for the slightly larger theoretical values than measurement in this figure, the reason is that cold clearance assumption is used for the neglection of thermal expansion. Prediction result is the smallest because it only considers the circumferential clearance backflow and neglects of those radial, tooth shape and tooth side. Experimental measurement, theoretical analysis and numerical simulation are in good agreements, testifying that proposed model and simulation are reliable.

6 Conclusion

- The profile design method of variable-pitch screw rotor with meshing clearance based on equidistant modification theory was created. Stable circumferential, radial, tooth side and tooth profile clearances from 5th to 1st stage were generated. Calculation model for backflow was improved to quantify their volume between different interstage clearances of meshing screw rotors, and the mechanism of inner backflow for variable-pitch screw vacuum pump was revealed.
- The four types of clearances had a certain impact on the backflow of vacuum pump. Generally, the larger the clearance was, the larger the backflow was. However, the circumferential clearance had the greatest influence, accounting for about 80% of the total backflow. The cross-sectional area and the length of circumferential clearance were important parameters affecting the backflow. The variable distance gradient design of circumferential clearance had practical significance in engineering.
- The backflow of three vacuum pumps with different clearances was increased with the increase of inlet pressure. However, the increment curves of the backflow between interstages were saddle shapes. In the 3rd stage variable distance compression section, the increment of the backflow was the smallest. The backflow between interstages also was increased with the increase of rotating speed. The backflow of the latter stage was significantly greater than that of the former stage, and the backflow of the 1st stage was the smallest.
- The consistency of theoretical calculation, numerical simulation and experimental test results shown that the backflow calculation model and numerical simulation method obtained in this paper had a good guiding role for the design of variable-pitch screw vacuum pump.

Nomenclature

x,y	Theoretical surface coordinates
x_r,y_r	Modified surface coordinates
δ	Predetermined clearance (°)
δ_1	Circumferential clearance between the rotor and stator (mm)
δ_2	Radial clearance between addendum surface of rotor and root surface of Another rotor (mm)
δ_3	Tooth side clearance between two concave surfaces of the rotor (mm)
δ_4	Tooth shape clearance between two convex surfaces of the rotor (mm)
R_A	Addendum circle radius (mm)
R_F	Root circle radius (mm)
R_d	Pitch circle radius (mm)
R_0	Base circle radius (mm)
β	Angle of the initial position (°)
A_i^j	Area of the jth interstage of the ith type clearance (mm^2)
S^j	The jth pitch lead (mm)
S^N	Pitch lead of exhaust end (mm)
β^j	The jth lead angle of screw (°)
B^j	The jth width of the addendum surface (mm)
$\tilde{M}_i^j$	Backflow of the jth interstage of the ith type clearance ($Pa \cdot m^3/s$)
$\tilde{M}_{ci}^j$	Couette backflow of the jth interstage of the ith type clearance ($Pa \cdot m^3/s$)
$\tilde{M}_{si}^j$	Orifice backflow of the jth inter-stage of the ith type clearance ($Pa \cdot m^3/s$)
v_i	Relative velocity (mm/min)
P^j	The jth interstage pressure (Pa)
x	Pressure ration between adjacent interstage
K	Gas heat capacity ratio
R	Gas constant ($J/(K \cdot mol)$)
μ	Gas molar mass (kg/mol)

Subscript

i	The ith type clearance, $i = 1, 2, 3, 4$
j	The jth interstage of pump, $j = 1, 2, ..., N$

The authors would like to acknowledge the financial support from the basic public welfare research project of Zhejiang Province in China (No. LGG19E050008), and the science and technology plan project of Taizhou city (No. 1803GY06).

Author contribution statement

All authors make equal contributions for manuscript.

References

[1] J. Wang, S.H. Wei, R.D. Sham, Design methodology of a new smooth rotor profile of the screw vacuum pump, Vacuum. **159**, 456–463 (2019)

[2] D. Pfaller, A. Brummer, K. Kauder, Optimized rotor pitch distributions for screw spindle vacuum pumps, Vacuum **85**, 1152–1155 (2001)

[3] S.W. Zhang, F. Zhao, J. Zhang, Z.J. Zhang, J. Han, Review and prospect of design ideas for the screw rotors in the oil-free twin-screw vacuum pumps, Vacuum **52**, 1–12 (2015)

[4] T. Ohbayshi, T. Sawada, M. Hamaguchi, H. Miyamura, Study on the performance prediction of screw vacuum pump, Appl. Surf. Sci. **169–170**, 768–771 (2001)

[5] K. Rabiger, T.M.A. Maksoud, J. Ward, G. Hausmann, Development of a finite volume model for the compressible gap flow inside a screw pump, Schriftenreihe Der Georg-Simon-Ohm-Fachhochschule Numberg. **30**, 2–19 (2005)

[6] Z.H. Fong, F.C. Huang, Evaluating the interlobe clearance and determining the sizes and shapes of all the leakage paths for twin-screw vacuum pump, Proc, Inst. Mech. Eng. C **220**, 499–506 (2006)

[7] V.M. Ryazantsev, V.V. Plyasov, Determining the forces on the screws in two-and three-bearing two-screw pumps, Russ. Eng. Res. **30**, 29–37 (2010)

[8] Z.H. Li, Q.S. Wang, G.D. Wang, C.Q. Chen, Z.W. Chen, D.Q. Zhang, Simulation of backflow characteristics for screw vacuum pump, Chin. J. Vacuum Sci. Technol. **35**, 1295–1299 (2015)

[9] S. Rane, A. Kovacevic, N. Stosic, Deforming grid generation and CFD analysis of variable geometry screw compressors, Comput. Fluids **99**, 124–141 (2014)

[10] H.Y. Xiao, Q.S. Wang, Y.Q. Wang, Modelling and simulation of gas transport in double screw vacuum pump, Chin. J. Vacuum Sci. Technol. **37**, 351–355 (2017)

[11] J.L. Straalsund, S.F. Harding, Experimental evaluation of advanced archimedes hydrodynamic screw geometries, J. Hydraulic Eng. **144**, 1–10 (2018)

[12] U. Zöllig, Dry-compressing screw vacuum pumps as enabler for demanding steel degassing processes, MPT Metall. Plant Technol. Int. **5**, 42–51 (2014)

[13] P. Abhay, M. Gerald, Performance of multiphase twin-screw pump during the period of wet-gas compression, SPE Prod. Oper. **33**, 68–72 (2018)

[14] Y.R. Wu, J.W. Chi, A numerical method for the evaluation of the meshing clearance for twin screw rotors with discrete tooth profile points, Mech. Mach. Theory **70**, 62–73 (2013)

[15] S. Dirk, K. Knut, B. Andreas, Operating performance of screw vacuum pumps, Vakuum in Forschung und Praxis **20**, 19–25 (2008)

[16] F. Zhao, S.W. Zhang, K. Sun, Thermodynamic performance of multi-stage gradational lead screw vacuum pump, Appl. Surf. Sci. **432**, 97–109 (2018)

[17] K. Kauder, D. Pfaller, Optimized design of screw-type vacuum pumps, VDI-Berichte **1932**, 161–176 (2006)

[18] D. Pfaller, A. Brummer, K. Kauder, Multi-criteria optimization of pitch curves for screw-type vacuum pumps, VDI-Fachtagung, VDI-Berichte. **2101**, 171–181 (2010)

[19] A. Burmistrov, L. Belyaev, P. Ossipov, Combined experimental and calculation study of conductance of roots pump channels, Vacuum **62**, 331–335 (2001)

[20] N. Stosic, I.K. Smith, A. Kovacevic, Vacuum and multiphase screw pump rotor profiles and their calculation models, VDI-Berichte **1932**, 53–66 (2006)

[21] S. Salikeev, A. Burmistrov, M. Bronshtein, Conductance calculation of channels in laminar gas flow regime at an arbitrary pressure difference, Vacuum **107**, 178–183 (2014)

[22] S. Salikeev, A. Burmistrov, M. Bronshtein, Conductance of slot channels formed by cylindrical walls: Monte Carlo calculations and experimental studies in the molecular gas flow regime, Vakuum in Forschung und Praxis. **25**, 34–38 (2013)

[23] S. Salikeev, A. Burmistrov, M. Bronshtein, Conductance calculation of slot channels in laminar gas flow regime at small pressure difference, Vacuum **99**, 303–306 (2014)

[24] S. Salikeev, A. Burmistrov, M. Bronshtein, Non-contact vacuum pumps: a general-purpose method for conductance calculation of profile slot channels, Vakuum in Forschung und Praxis **26**, 40–44 (2014)

[25] Y.X. Zhang, Q. Tang, Z.W. Jiang, Z.H. Lim, Design of screw tooth profile based on backlash and design method of forming cutter, J. Mech. Eng. **50**, 48–57 (2014)

[26] D.A. Da, Vacuum design manual, National Defense Industry Press (2004)

Cite this article as: L. Zhang, Y. Zhang, Z. Chen, Effects of stable clearances on backflow in the variable-pitch screw vacuum pump, Mechanics & Industry **22**, 46 (2021)